Journal of Neuroscience Methods 397 (2023) 109921

Contents lists available at ScienceDirect

Journal of Neuroscience Methods

journal homepage: www.elsevier.com/locate/jneumeth

Wide field block face imaging using deep ultraviolet induced autofluorescence of the human brain

Srinivasa Karthik [a,b,*], Jayaraj Joseph [b], Jaikishan Jayakumar [c,d], Rahul Manoj [a,b], Mahesh Shetty [c], Mihail Bota [c], Richa Verma [c], Partha Mitra [d,e], Mohanasankar Sivaprakasam [a,b,c]

[a] Healthcare Technology Innovation Centre, No. 1, 5th Floor, 'C' Block, Phase-II, IIT Madras Research Park, Kanagam Road, Taramani, Chennai 600113, India
[b] Department of Electrical Engineering, Indian Institute of Technology Madras, IIT P.O., Chennai 600036, India
[c] Sudha Gopalakrishnan Brain Centre (SGBC), Indian Institute of Technology Madras, NAC Building 1, Stilt Floor, IIT P.O., Chennai 600036, India
[d] Center for Computational Brain Research, Indian Institute of Technology Madras, IIT P.O., Chennai 600036, India
[e] Cold Spring Harbor Laboratory, 1, Bungtown Road, Cold Spring Harbor, New York 11724, United States

ARTICLE INFO

Keywords:
Block face imaging
Histology
Adult human brain
Autofluorescence
Ultraviolet-C
Large field of view

ABSTRACT

Background: Imaging large volume human brains at cellular resolution involve histological methods that cause structural changes. A reference point prior to sectioning is needed to quantify these changes and is achieved by serial block face imaging (BFI) methods that have been applied to small volume tissue (~1 cm^3).
New method: We have developed a BFI uniquely designed for large volume tissues (~1300 cm^3) with a very large field of view (20 × 20 cm) at a resolution of 70 μm/pixel under deep ultraviolet (UV-C) illumination which highlights key features.
Results: The UV-C imaging ensures high contrast imaging of the brain tissue and highlights salient features of the brain. The system is designed to provide uniform and stable illumination across the entire surface area of the tissue and to work at low temperatures, which are required during cryosectioning. Most importantly, it has been designed to maintain its optical focus over the large depth of tissue and over long periods of time, without readjustments. The BFI was installed within a cryomacrotome, and was used to image a large cryoblock of an adult human cerebellum and brainstem (~6 cm depth resulting in 2995 serial images) with precise optical focus and no loss during continuous serial acquisition.
Comparison with existing method(s): The deep UV-C induced BFI highlights several large fibre tracts within the brain including the cerebellar peduncles, and the corticospinal tract providing important advantage over white light BFI.
Conclusions: The 3D reconstructed serial BFI images can assist in the registration and alignment of the microscopic high-resolution histological tissue sections.

1. Introduction

High quality histology still remains the gold standard for our basic understanding of the brain. However, histological pipelines involve a number of steps which potentially distort or warp the tissue. The end goal in understanding the microstructure of the whole brain is the entire and precise 3D histological reconstruction from 2D high quality histological sections (Pichat et al., 2018). This process involves annotation and mapping 2D histological data with macroscopic neuroanatomical structures, generally obtained from standard volumes derived from brain atlases of different modalities (Amunts et al., 2013; Ding et al., 2016; Mai et al., 2015). Other standardized volumes of the whole human brain, acquired with Magnetic Resonance Imaging (MRI), have also been created (Collins et al., 1994; Evans et al., 1992; Holmes et al., 1998; Mazziotta et al., 1995; John et al., 1995; Talairach and Tournoux, 1988). In addition, many groups aim to create a comprehensive 3D atlas of the

Abbreviations: BFI, Block Face Imaging; FoV, Field of View; LED, Light Emitting Diodes; MRI, Magnetic Resonance Imaging; UoD, Uniformity of Distribution; UV-C, Ultraviolet C.

* Correspondence to: Sudha Gopalakrishnan Brain Centre, NAC Building 1, Stilt Floor, Indian Institute of Technology Madras, Chennai 600 036, India.
E-mail address: karthik.s@htic.iitm.ac.in (S. Karthik).

https://doi.org/10.1016/j.jneumeth.2023.109921
Received 24 March 2023; Received in revised form 26 June 2023; Accepted 13 July 2023
Available online 17 July 2023

whole human brain at cellular resolution(Amunts et al., 2020, 2013; Ding et al., 2016). The problem in generating such a high resolution atlas volume is the availability of serial sections from a single large volume human brain. One approach for simplifying the process is to combine the advantages of high granularity of histological data with the macro-level anatomical information, of the whole human brain (Alegro et al., 2016) or parts of it (Alho et al., 2018; Annese et al., 2006; Choe et al., 2011; Lebenberg et al., 2010). Such approach has fundamental limitations, including a) potential distortions that can be linear or non-linear, which may occur during sectioning and chemical handling of the tissue (Pichat et al., 2018), b) differences in spatial resolution between MRI (~mm) and histology (<μm), and c) sections of large brains may require to be cut into smaller blocks and later registered as a single unit. The problem of sub blocking a brain into smaller units can be solved with the use of a cryomacrotome which is capable of sectioning large volume tissues. One obvious solution to a) and b) is the use of block face imaging (BFI), where the surface of the cryoblock can be imaged at a sufficiently reasonable resolution that can be used to generate a reference volume (Appel et al., 2013). BFI is applied prior to cryosectioning. The 3D volume from the block face images acts as a reference to quantify any distortions or warpings that may occur to the tissue due to the cryosectioning or the staining processes. This is particularly important in large volume tissues such as the human brain where the probability of sectioning artefacts occurring is much greater due to the large surface area (Mancini et al., 2020). Hence there is a significant need for the development of a block face imaging system that is specific to large volume tissues. In particular, such a system needs to capture images at a high enough resolution yet capture a large field of view.

In this paper, we describe a BFI system that is capable of optically imaging large volume tissue (200 mm × 150 mm) embedded in an embedding compound to form a cryoblock, at a resolution of 70 μm/pixel. In addition, our BFI is stable enough to resolve the significant changes in the focal plane over large depths of tissue block (~ 7 cm). The set of block face images of the cryoblock provides a way of capturing and quantifying changes related to cryosectioning and staining and thus can serve as an alignment template when the sub-cellular level high-resolution images post staining, are co-registered against the MRI or other reference volumes of different modalities.

We have deployed a high throughput experimental and computational pipeline to study the human brain with high resolution histology and other modalities, such as MRI. Our high throughput histology pipeline is shown in Fig. 1, and includes the following steps: brain extraction, cryoprotection, freezing, cryosectioning, specific histological staining including immunohistochemistry. The outputs of this pipeline are 2D brain sections which are then digitized by sub-cellular level high-resolution imaging (0.5 μm per pixel in plane resolution), and most importantly, the output of this pipeline is the computational 3D reconstruction from high-resolution 2D images. These output volumes require registration to the relevant reference volumes such as known atlases or in skull MRI. The histology pipeline involves cryoprotection of the brain in gradient sucrose and freezing the block, followed by cryosectioning. Block face Imaging (BFI) is performed during cryosectioning, which involves capturing serial sub-millimeter resolution images of the exposed surface of the cryoblock.

Several approaches have been performed to optically image biological tissue prior to, or as an alternative to sectioning. Optical alternatives that can acquire cellular-scale images directly from tissue surfaces without micro- or cryosectioning include structured illumination (Neil et al., 1997) conventional reflectance and fluorescence confocal microscopy (Dobbs et al., 2015), multi-photon imaging (Tang et al., 2012), spectrally encoded confocal microscopy (Kang et al., 2013), stimulated Raman microscopy (Orringer et al., 2017), light-sheet microscopy (Bouchard et al., 2015; Lu et al., 2019) and optical coherence tomography (Gabriele et al., 2011). While all appear promising, they are expensive, and most can only be applied to small pieces of tissue.

Other approaches that are applied directly onto the tissue block include scanning electron surface microscopy (Denk and Horstmann, 2004; Lipke et al., 2014; Starborg and Kadler, 2015), which provides nanometer resolution on very limited size samples, ultraviolet surface excitation (Guo et al., 2019b; Kasaragod et al., 2021), and brightfield fluorescence (Roy et al., 2009; Takaishi et al., 2014; Wilson et al., 2008) which can be applied along with other optical clearance methods and fluorophores to study at the sub-micron images of the tissue. However, histological staining methods still remain the gold standard of neuroanatomy, particularly for studying multiple facets of the brain such as cells, fibres, specific proteins, genes etc. BFI itself is not a replacement to

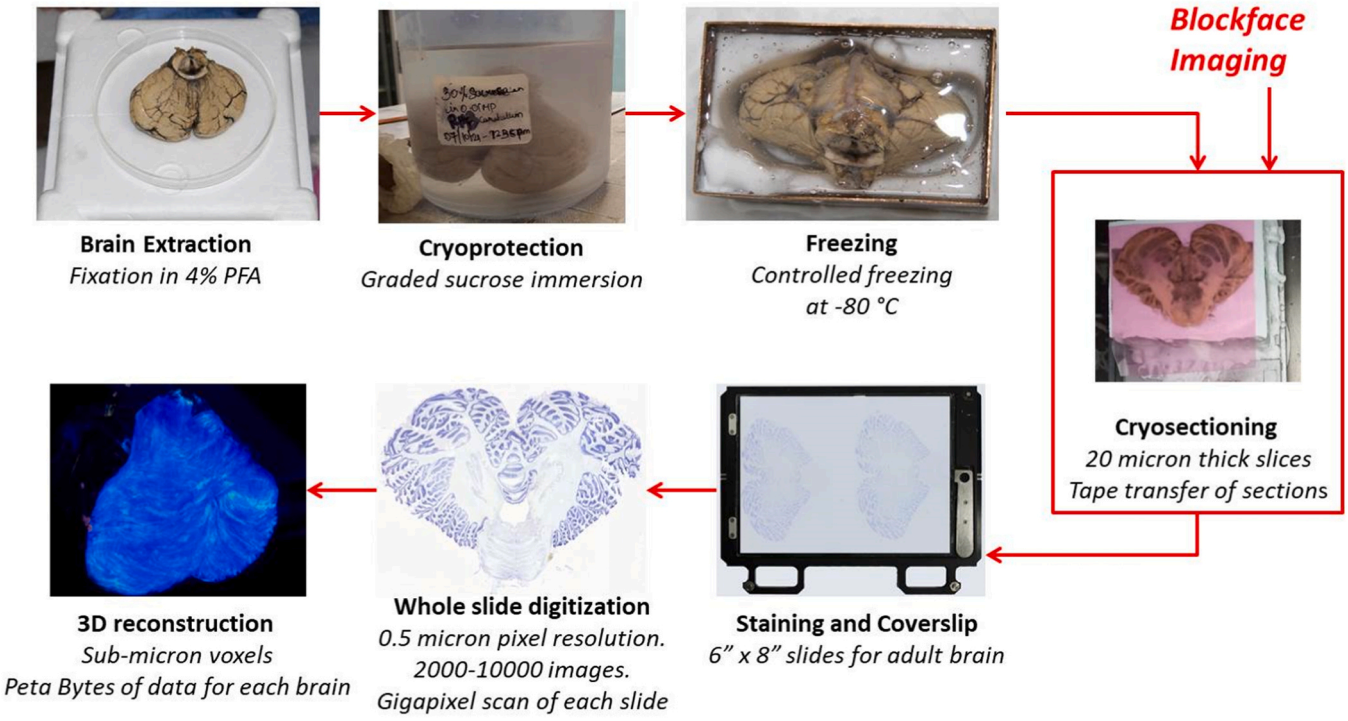

Fig. 1. Main steps involved in our histology pipeline. Block face images are obtained during the cryosectioning stage.

the gold standard as it images unstained and non-modified tissues. Although brain atlas mapping based on BFI using macro images and microscopy, where BFI was used in conjunction with microscopy analysis are explored in (Ishii et al., 2021; Tajika et al., 2017), these methods again have limitations in use of large samples that do not fit in standard histological slide sizes, such as of the adult human brain. In addition, BFI is a snapshot imaging technique, which saves considerable time as compared to scanning based techniques, especially for large size tissues.

The BFI described here also uses a deep ultraviolet (254 nm in our case) excitation light that is invisible to the camera and thus is isolated from the ambient lighting. The choice of wavelength chosen is based on the fact that formalin fixed brain tissue inherently fluoresces under deep ultraviolet light and this autofluorescence is exhibited differently by the various components of the brain tissue. Conventionally, BFI has been used to image the block face in white light and using staining methods when used with UV (Fereidouni et al., 2021; Guo et al., 2019a). Our use of UV-C produces autofluorescence that highlights the contrast particularly of the white matter tracts even in unstained and non-modified tissues. This difference in autofluorescence exhibited by the various components of the brain tissue maybe due to the constituents such as lipofuscin, lipids, amino acids and metabolic products like NADPH which differ between white matter and gray matter (see table 1 of Croce and Bottiroli, 2014).

The requirement is to effectively design a BFI system to a) image a large FoV, such as the human brain tissues b) image at a high resolution at the large FoV, and most importantly c) retain stable camera focus over large depth (~7 cm) corresponding to large volume tissues. We also introduce a novel procedure of imaging at UV-C which highlights important components in a differential manner.

2. Methods

2.1. Requirements

Our goal for the BFI is to capture images of the large volume tissue block face at an intermediate resolution between MRI and histology. Unlike previous work, we did not aim for subcellular level imaging that can potentially replace histology. The large volume cryoblock comes with a caveat that any given system has to image a large enough field of view (FoV) yet maintain sufficient resolution. More importantly, our application involves human brain sections (ranging from developing stages to the adult brains) that are considered non-standard, i.e. do not fit on 75 × 25 mm slides. Hence, we designed our setup to be adaptable to capture block face images of multiple non-standard slide dimensions ranging from the double slide set up (75 × 50 mm slides) up to a maximum of 150 × 200 mm slides.

The imaging system needs to have a depth of focus narrow enough to accommodate the plane of the exposed block face, yet account for surface micro irregularities. One important problem is that the large volume blocks can be very thick, that is the difference in depth between the first and the last section can be as much as 7 cm apart. This poses a challenge for any fixed BFI system as the focus and magnification must account for exposed block face moving away from the camera as tissue sections of specified thickness are progressively sectioned and removed. This is solved by coupling the BFI system with the knife holder assembly.

The developed BFI is based on a specific wavelength-based diffused illumination in the UV-C range which elicits natural tissue fluorescence. Therefore the source light intensity has to be optimized by factoring the sensitivity of the imaging sensor to the tissue fluorescence signal. Other factors include the placement of the camera and the illumination system to be unobtrusive to the mechanical process of cryosectioning, and with

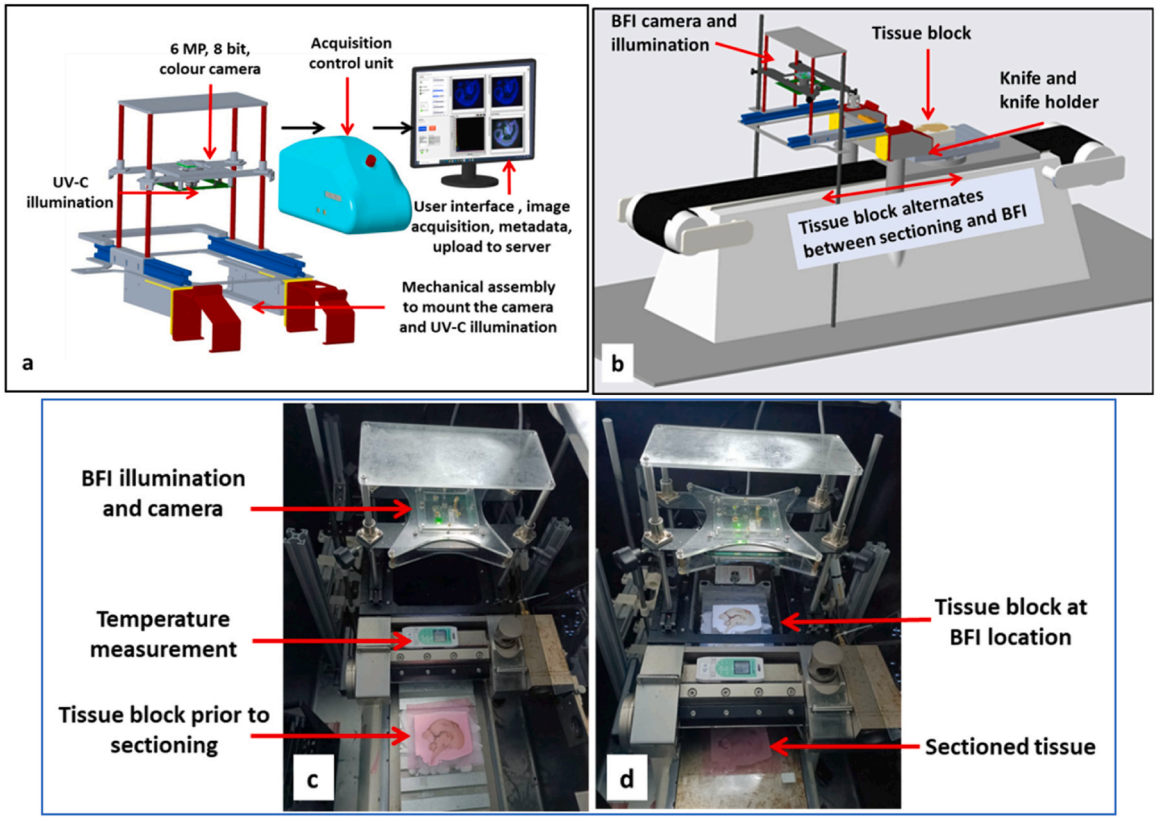

Fig. 2. a) The BFI architecture showing the UV-C illumination and camera, the acquisition control unit to initiate a BFI capture, and the user interface to see the captured BF image. b) The BFI setup mounted on the knife holder of the cryomacrotome (is shown rotated by 90° with respect to Fig. 2a) c) shows the setup inside the cryomacrotome showing the positioning of the tissue block just before sectioning using the tape transfer method d) the conveyor belt of the cryomacrotome moves the tissue block towards the blade and onwards to the location where the exposed block face will be imaged.

unhindered access to the tissue. The entire BFI setup has to be either retractable, to allow access to cryosectioning, or the setup needs to be stationary but spatially separated from the sectioning part. The latter method is implemented here with the tissue block moving towards the BFI setup. The conveyor stoppage tolerances introduce an additional problem of pixel level shifts in the block location within the captured FoV, across the captured images. To solve this, alignment markers (fiducial markers) were placed on the base of the cryosectioning chuck to align the serial block face images during image processing. The overall system also needs to work in cold temperatures required for cryosectioning (−20 to −30 °C).

2.2. System design & architecture

The cryosectioning process uses a cryomacrotome (Leica 3600XP) to section large volume blocks where the knife holder module moves downward in set steps to section the tissue. The cryomacrotome includes a horizontally moving conveyor belt to alternately move the cryoblock between cryosectioning and the BFI setup. The BFI system has three major components: a) the camera and illumination output systems that are mounted on the knife holder assembly of the cryomacrotome, b) the control unit hardware system of the UV-C illumination and c) a custom developed software developed on LabVIEW environment (National Instruments Inc, India) for image acquisition and storage. The architecture of the BFI system and the mounting of the BFI assembly are shown in Fig. 2.

2.2.1. Camera

We used a light weight 6 Megapixel, 8-bit, color camera (UI-3881LE-C-HQ, IDS Imaging Development Systems GmbH, Germany). A manually adjustable, 8 mm focal length, 14 mm aperture lenslet was used with this camera. No pixel binning or frame averaging was performed and a single BF image was captured for every tissue section. The camera and the illumination light emitting diodes (LEDs) were light enough to be mounted on the knife assembly without introducing any vibrations or movement that could affect the cryosectioning itself. The focus setting of the camera was adjusted using high-resolution target patterns (USAF resolving power test target 1951, Edmund Optics). This is done as a one-time focus routine for each sample prior to the start of cryosectioning. Our set up is designed in a way that the working distance and focus of the camera can be adjusted to maximize the FoV of the imaging. In other words, we can utilize the same camera system for multiple block sizes (sections sizes that can fit on 75 × 50 mm to the large 150 × 200 mm slide formats). Also, the camera is insensitive to deep ultraviolet wavelengths thereby reducing potential artefacts from the excitation light source.

2.2.2. Illumination

The exposed cryoblock face was illuminated by an array of eight LEDs placed around the camera in a circular arrangement which provided the block face with an illumination uniformity of distribution (UoD) of 70 %. Each LED was driven at 5 W of power and is turned on for 2 s. The camera's sensor is insensitive to UV-C and thus prevents image saturation from any specular reflection of source light. The emission of interest from the tissue fluorescence lies in the visible region wavelengths and has low intensity, requiring optimum exposure duration of 250 ms, and is exposed towards the end of the 2 second illumination period. In addition, a broadband white light source was also provided for positioning the cryoblock correctly in the cryomacrotome (turned off during BFI capture).

2.2.3. Mechanical assembly of the system

The camera and illumination system were mounted and secured on the cryomacrotome's knife holder assembly. The computer controlled cryomacrotome can be programmed to advance the knife holder assembly by a distance equal to a preset thickness (in our case 20 μm). The securing of the entire BFI setup on this assembly implies that the BFI system also advances along with the knife holder assembly. The obvious advantage of such an arrangement is that as the newly exposed block face recedes away from the camera during cryosectioning, the BFI system also advances by the same distance equal to the section thickness, thereby compensating and maintaining a constant plane of focus and FoV. This negates the need for any periodic manual readjustment of camera focus. The arrangement, mounting and securing of the BFI setup to the knife holder assembly of the cryomacrotome is shown in Fig. 2.

2.2.4. Control unit

We designed an acquisition control unit placed outside the cryomacrotome which electronically controls the precise timing of UV-C LED illumination and the camera exposure.

2.2.5. Software

Our image acquisition set up is controlled by a custom designed user interface software developed using the LabVIEW platform. The software is designed to be user friendly and performs image acquisition, storage to a central server along with associated metadata such as section number, date, time and other parameters including exposure, gain and gamma correction. The latter parameters can also be changed prior to cryosectioning. In addition, the software and the image acquisition systems provide real-time views of the block under a broadband white light source, which can be used for quality checks, alignment, positioning and focussing. The user interface also allows the operator to preset the UV-C LED array power-on duration and the camera exposure duration.

The position of the block face in the camera's field of view can be programmatically controlled, but there is a tolerance of + /- 5 mm in the mechanically operated cryomacrotome's conveyor. Therefore, the location of the block face in the imaging FoV changes between sections. To compensate for this, and to ensure alignment between all BFI images, we placed square reference fiducial markers at two corners of the cryosectioning chuck. These square markers fluoresce under UV-C, and can be used to align the images.

We have also introduced a safety feature where the UV-C LED light source can only be turned on if the cryomacrotome door is closed, thus preventing any UV-C exposure to the operator. In addition, the duration of illumination is kept short (2 s), just enough to capture an image.

2.3. Sample preparation

We tested our system on an adult human cerebellum and brainstem block. BFI was tested on its ability to obtain images from large format tissues without the need for frequent focus adjustments. All the procedures for processing the human cerebellum and brainstem block were approved by the institutional ethics committee of Indian Institute of Technology Madras. Briefly, the sample was prepared from an ex-situ perfusion protocol where the brain was perfused with 0.01 M phosphate buffer followed by 4 % paraformaldehyde solution through the bilateral carotid arteries. The whole brain was then immersed in 4 % paraformaldehyde. The cerebellum, together with the brainstem, block were resected from the entire brain by separation of the superior cerebellar peduncles. The block underwent cryoprotection in increasing gradients of sucrose (10–30 %) before being embedded and frozen in an embedding compound (Tissue Freezing Medium, Leica Biosystems, USA) as a cryoblock, using isopentane in dry ice bath. Block cryosectioning was performed on the large format cryomacrotome (Leica 3600 XP) using the modified tape transfer technique (Pinskiy et al., 2015) along with BFI. After cryosectioning, sections underwent histological staining procedures including thionin staining with cresyl violet (Nissl stain), and were digitized at 0.5 μm per pixel (in plane resolution).

3. Results

3.1. Functional performance and reliability of the developed BFI system

The BFI system was built and integrated into a large format cryomacrotome. Its functionality and performance were evaluated on

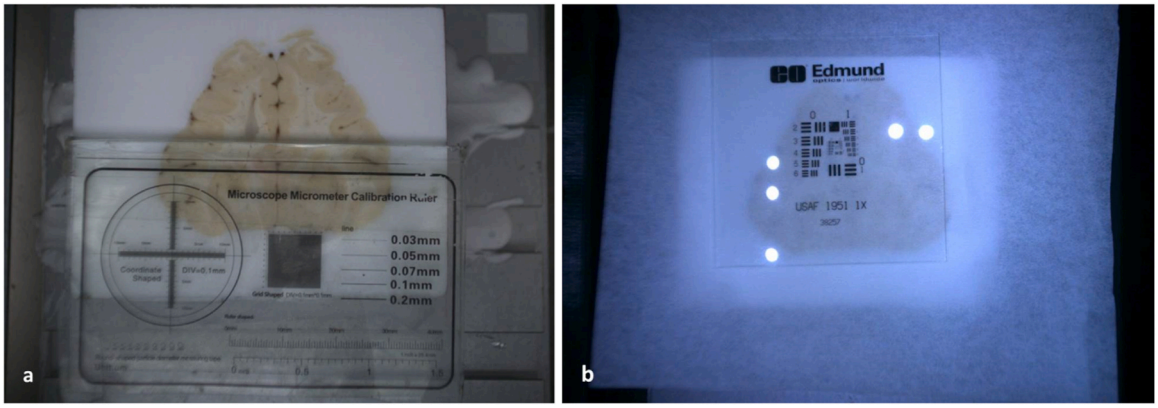

Fig. 3. One time lens focus adjustment of the BFI system's camera performed using a) microscope micrometer calibration ruler (coarse) and b) 1951 USAF resolution target (fine). The focus adjustments were performed under broadband white light source.

sectioning an adult human brain cerebellum and brainstem with surface dimensions of 105 mm × 80 mm and depth of 60 mm. Prior to sectioning, the lens was precisely adjusted for focus; initially a coarse adjustment was done with a microscope micrometer calibration ruler (Fig. 3a), followed by fine scale adjustment using a USAF 1951 resolution target (Edmund Optics) (Fig. 3b). For this particular large volume brain tissue cryoblock, the camera FoV after focus adjustment was 172 mm × 116 mm and the spatial in plane resolution of the captured BF images was 70 μm/pixel. We captured a total of 2995 sections in a serial manner during the cryosectioning procedure. The average time taken by the system to capture one block face section was 10 s, which includes the blade and the cryochuck movement resets. The BFI system operated in tandem with cryosectioning with no failures and was highly reliable across longer time periods taken for the entire cryosectioning process, which was performed over 15 days (at an average rate of 200 sections per day) at low ambient temperatures ranging from −20 to −30 °C. There was no drift or loss in the illumination across the entire duration, while the spatial intensity being maintained at a uniform rate (UoD = 70 %). There was no readjustment of the camera's focus and the focus was maintained throughout the duration of the cryosectioning.

We have performed measurements of incident optical power of the UV-C illumination at the surface of the block using an optical power meter (843-R, Newport Corporation, UV sensor) and were found to be 13 μW/cm^2. In our BFI, the illumination exposure is two seconds, which constitutes a dosage of 26 μJ/cm^2. This is far below the limits of UV-C dosage that can cause damage to biological tissues which is 2–2.5 J/cm^2 (Scientific Committee on Emerging and Newly Identified Health Risks: SCENIHR, 2012), 200 mJ/cm^2 specifically for nerve damage

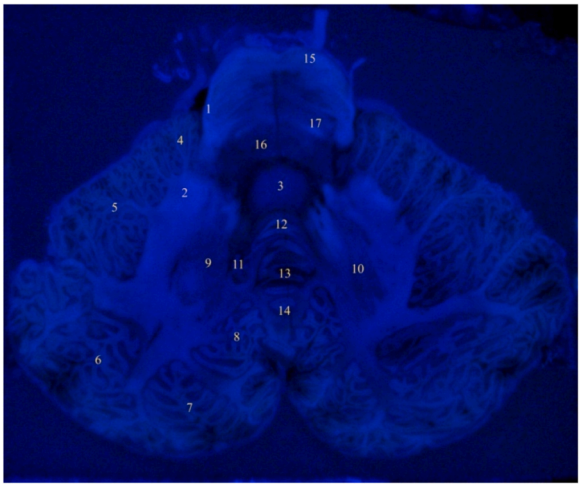

Fig. 5. BF image of a horizontal section of the adult human cerebellum and brainstem. Regions 1–17 labelled as: 1. Inferior cerebellar peduncle; 2. Middle cerebellar peduncle; 3. Fourth ventricle; 4. Anterior lobe of the cerebellum; 5. Simple lobule; 6. Ansiform lobule crux I; 7. Ansiform lobule crux II; 8. Paraflocullus; 9. Deep cerebellar nuclei; 10. Dentate nucleus; 11. Tonsil; 12. Nodulus; 13. Uvula; 14. Pyramis; 15. Corticospinal tract; 16. Pons nuclei; 17. Medial lemniscus. The annotations of neuroanatomical parts were made according to (Naidich et al., 2009), and (Schmahmann et al., 1999).

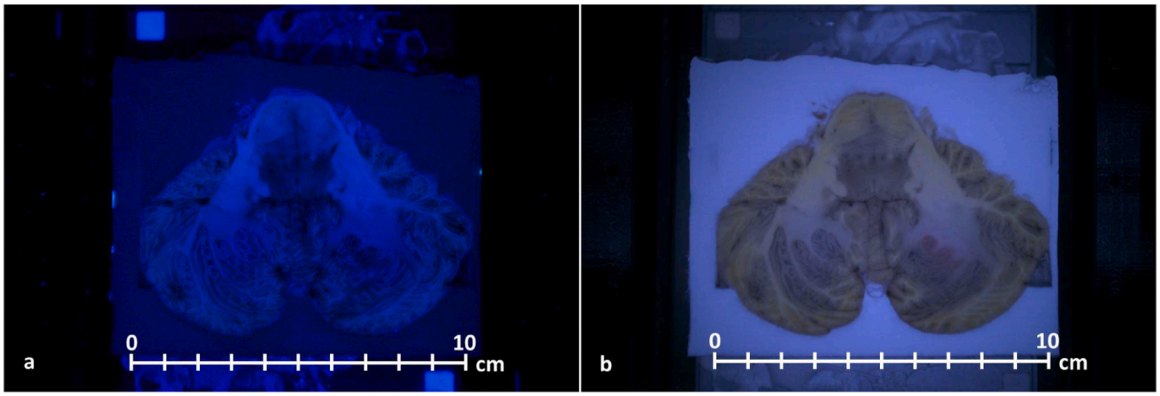

Fig. 4. Block face image of the exposed cerebellum and brainstem section of a human adult brain section number 1276 under a) deep ultraviolet illumination and b) broad band white illumination. Both images show a clear tissue - embedding compound boundary. The deep ultraviolet imaging shows the captured autofluorescence of the block. The fiducial makers on the top left and bottom right corners which fluoresce under UV-C illumination can be noted.

(Yoshiyama et al., 2023) and a more conservative reported value of 6–10 mJ/cm^2 for biological tissues (Sliney et al., 2021). The safety of the operator is also ensured as the BFI setup is completely enclosed within the cryomacrotome.

An example of a block face image under the UV-C and broadband white light illumination is shown in Fig. 4. Our system can capture images in great detail, which aids in further neuroanatomical processing. The example section shown in Fig. 4 is a horizontal (transverse) human brain section at the level of the pons and the middle cerebellar peduncle. The biological autofluorescence of the cerebellum and brainstem block under the deep ultraviolet illumination highlights many key anatomical features of the cerebellum with the prominent white matter tracts showing marked increase in brightness. We have identified and annotated these key features as shown in Fig. 5. The deep ultraviolet illuminated BFI elicits strong fluorescent signal in the white matter (fibre tracts), with the strongest signals highlighted in (1) the inferior cerebellar peduncle, (2) the middle cerebellar peduncle, (15) the corticospinal tract and in (17) the medial lemniscus.

3.2. Quantification of difference in spectral characteristics between white and gray matter

To perform a spectral characterization of the substructures of the brain tissue, we imaged the tissue with a hyperspectral camera (MQ022HG-IM-SM4×4-VIS3, Ximea, 460–600 nm, 16 bands) under UV-C and white light. Regions of white and gray matter were visually identified and corresponding regions of interest (RoI) were marked (depicted on white light image in Fig. 6d). To obtain a reference, an RoI was marked on the background region as well. The hyperspectral camera used had a snapshot mode of acquisition where images for all 16 wavelengths appear at once, and any RoI set is replicated to all wavelengths. The mean pixel intensity value of the RoI was obtained for each wavelength. The pixel intensities of white and gray matter were normalized with background and plotted (Fig. 6a for UV-C illumination, Fig. 6b for white light illumination). Fig. 6a and 6b clearly show a larger difference in background normalized irradiance between white and gray matter, with white matter being higher. This is especially true in the lower, blue wavelengths where most of the autofluorescence under UV-C exists. To quantify and compare, we computed the contrast difference (WM-GM/BG), which is the difference between normalized white and gray matter divided by the background and has been plotted in Fig. 6c. Autofluorescence from UV-C illumination provides about five times higher contrast between white and gray matter in the lower, blue wavelengths. This clearly shows the advantage of block face imaging over broadband white light imaging in terms of delineation of substructures.

3.3. Comparison with cellular level high resolution histology

Figs. 4 and 7 show the comparison between the BFI images under deep ultraviolet, broadband white illumination and high resolution digitized image of a Nissl stained histological section. The broad band white illumination BFI shows the separation of the white and gray matter where the gross structural details are visible, but the deep ultraviolet fluorescence also highlights the prominent white matter tracts which can then be used as an intermediate reference to the cellular-level high-resolution brightfield histological images.

We have compared the sharpness of the boundaries between the actual tissue and the embedding compound in the BFI to the high resolution histology section. Fig. 7 shows the clear distinction of tissue-embedding compound boundary, which is comparable to the tissue boundary observed in the down sampled Nissl stained cellular level high resolution image of the same tissue section.

In addition, the comparison between the BFI and the histological section provides an insight into the structural changes due to sectioning and staining process. In order to compare the two images which are of different resolution, we have downsampled (1/32x) and centered the Nissl stained images to match the BFI image. The two images now

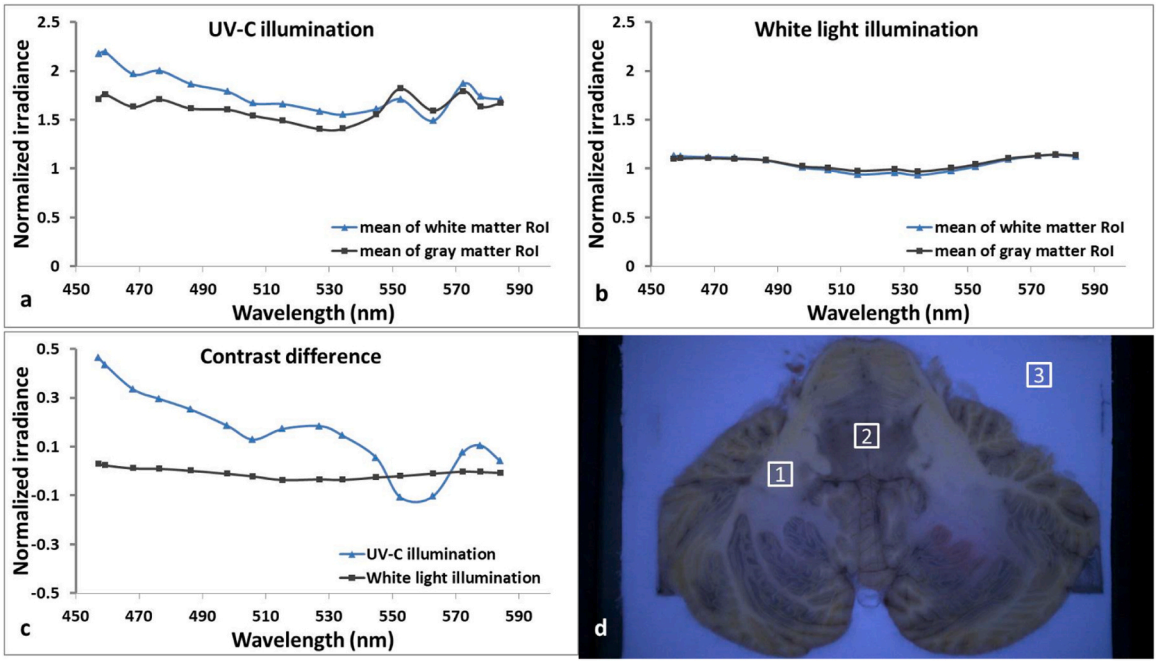

Fig. 6. Quantification of difference in spectral output between white and gray matter using a hyperspectral camera. a) plot of mean value of region of interest (RoI) for white matter and gray matter normalized to background (WM/BG, GM/BG), plotted across all wavelengths under UV-C illumination. b) plot of mean value of RoI for white matter and gray matter normalized to background, plotted across all wavelengths under white light illumination. c) comparison of the contrast between white matter and gray matter (WM-GM/BG) between UV-C and white light illumination indicating five times higher contrast in the lower wavelength autofluorescence under UV-C as compared to white light. d) the RoIs used for obtaining mean irradiance values – 1-white matter, 2-gray matter, 3-background, depicted on a white light image.

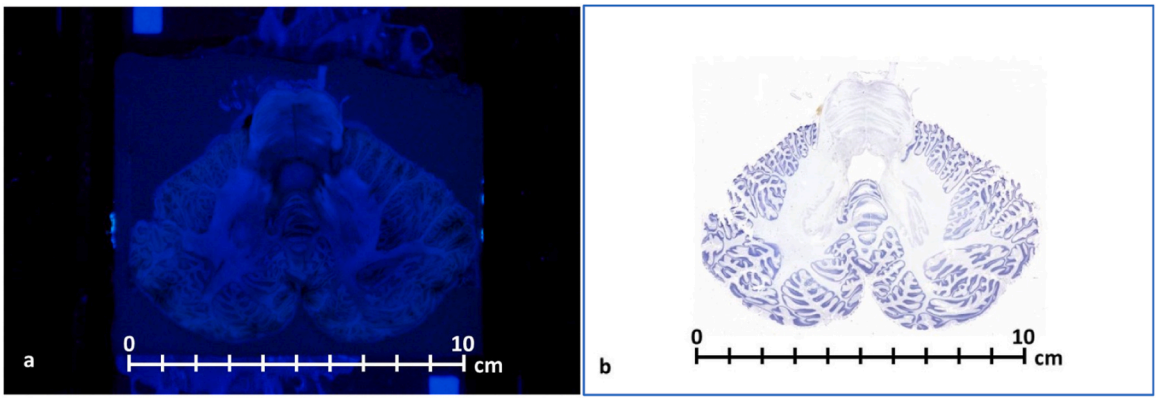

Fig. 7. Horizontal section of the human cerebellum and hindbrain (section number 1579, at the level of pons). a) BF image of 172 × 116 mm FoV. b) Down sampled image of the digitized Nissl stained section, appended by white pixels to form a frame size of 172 × 116 mm.

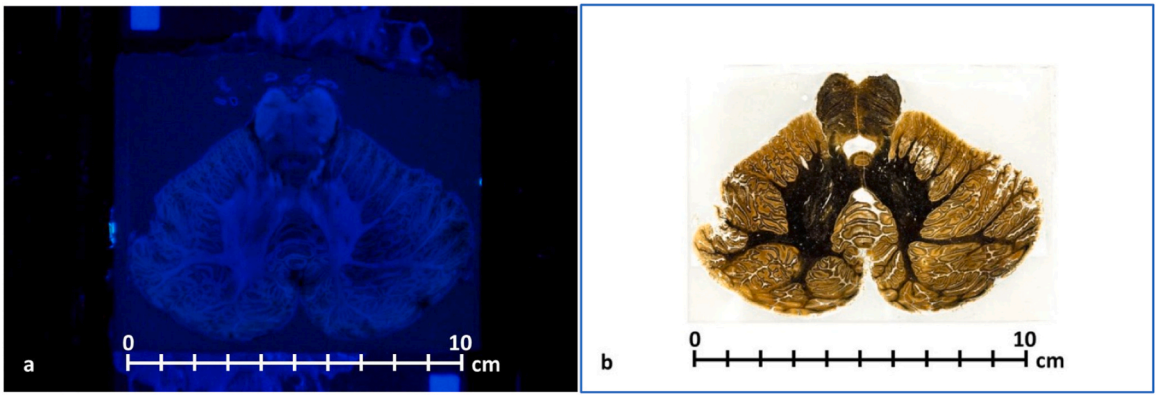

Fig. 8. Horizontal section of the human cerebellum (section number 1728). a) BF image of 172 × 116 mm FoV. The BFI highlights the white matter tracts which correlates to the myelin stained regions b) Down sampled image of the digitized myelin stained section, appended by white pixels to a frame size of 172 × 116 mm. The two images demonstrate the close correspondence of the bright fluorescence observed with the UV-C BFI and the darkly stained silver myelin of the histology section.

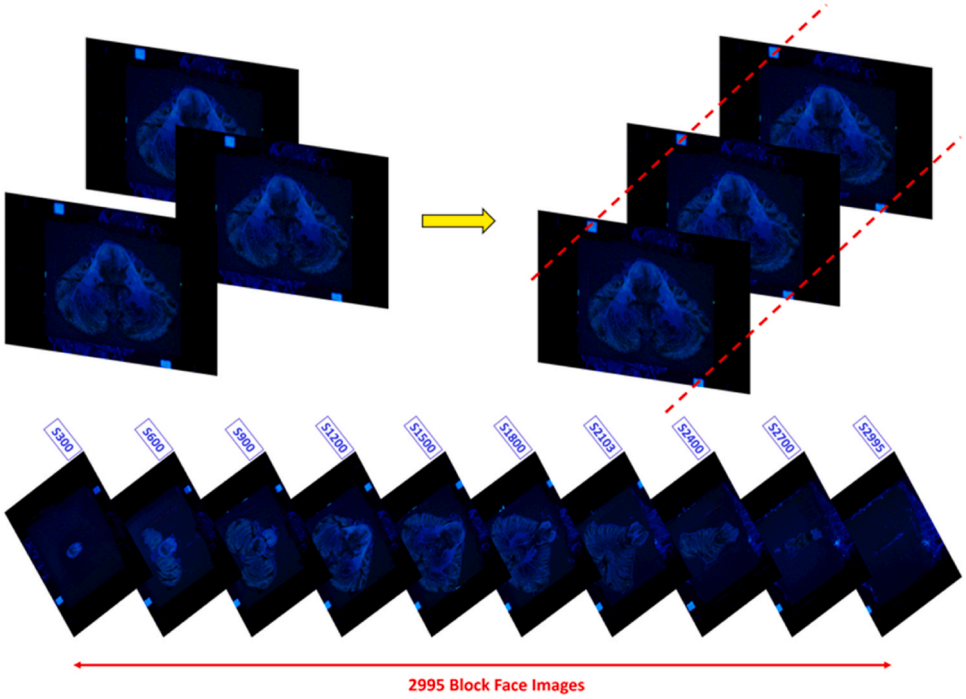

Fig. 9. Top: Fluorescent fiducial markers used to compensate for shifts due to conveyor belt stoppage tolerances. Bottom: A representation of one out of every three hundred sections from the captured BFI images post-alignment.

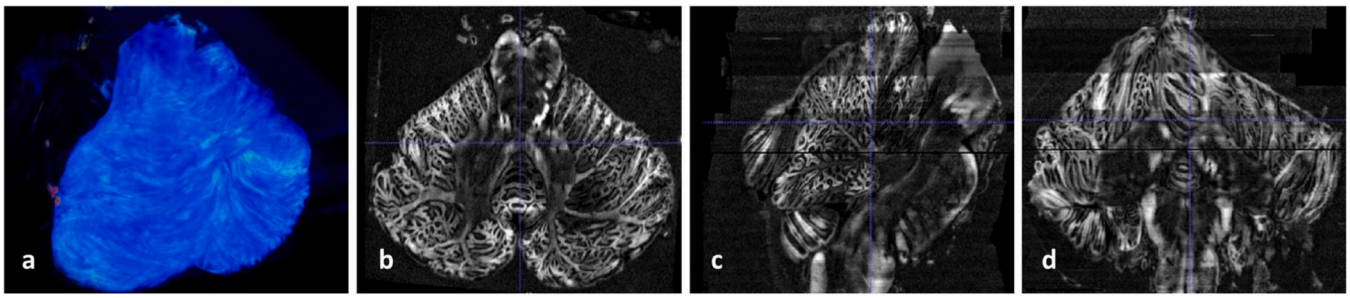

Fig. 10. 2D snapshots of the 3D volume reconstruction using all the BF images. (a): Complete view of the 3D volume reconstruction. (b): The transverse section obtained from the 3D reconstruction, which is the original plane of imaging. (c): A 2D snapshot of a sagittal plane obtained from the 3D volume reconstruction. The right side is the front of the brain. (d): A 2D snapshot of a coronal plane obtained from the 3D volume reconstruction.

correspond to the BFI FoV of 172 × 116 mm spatially, which allows us a direct comparison (Fig. 7). This comparison allows us to estimate any linear or non-linear diffeomorphic changes that the tissue may undergo during the cryosectioning and subsequent staining process, and in this particular example, the resulting distortions are minimal.

The UV-C BFI shows a greater contrast to white matter tracts. As shown in Fig. 8a, our BFI images show that the autofluorescence correspond very closely to the white matter tracts as shown in the myelin stained histology section in Fig. 8b. The darker silver myelin staining correlates with the corresponding regions in the BFI image with higher fluorescence intensity.

3.4. Section to section image alignment and volume generation from BF images

In order to facilitate section to section alignment of the serially captured BFI images, we have used features within the BFI images in addition to the square fluorescent fiducial markers. The two fluorescent fiducial markers (1 × 1 cm squares) were placed on the cryochuck of the cryomacrotome. These were used to align the tissue position in the FoV to compensate for planar shifts that occur due to conveyor stoppage tolerances. The fiducial markers were easily detected due to their fluorescence under deep ultraviolet light and the centers of these markers aligned (Fig. 9). Serial BFI images were stack aligned using the scale invariant feature (SIFT) program within the ImageJ/FIJI image processing environment (Lowe, 2004) using linear alignment as references to align consecutive images. Since the in-plane (x, y) resolution of the images was different to the section thickness (z), the images were z-scaled appropriately by linear interpolation to generate the 3D volume as shows in Fig. 10a. This 3D reconstructed isotropic volume also allows us to digitally section the block in other planes of sectioning as shown in Fig. 10c and 10d with the original plane of sectioning shown in Fig. 10b.

The 3D reconstruction can then be used to visualize the trajectory of the major white matter pathways. In Fig. 11 we show the segmentation of, medial lemniscus and superior cerebellar peduncle marked in red and green respectively and the reconstructed 3D trajectories when the BFI images were reconstructed.

4. Discussion

This work describes a BFI system that captures serial block face images of large volume cryoblocks as a structural reference to quantify the potential distortion of the reconstructed cellular level high resolution images of stained tissues. Though BFI at better resolution has been implemented on smaller tissues, developing a system uniquely for large format tissues presented its own challenges. Our main focus was to maximize the FoV to accommodate large tissue sizes at the expense of in plane resolution which still resulted in 70 μm/pixel, which was better than our MRI. The BFI system is designed to be mounted on the knife holder assembly of the cryomacrotome so that the distance between the camera and the block face is constantly maintained. This also means that the BFI system has to be as light as possible to avoid any mechanical loading of the knife holder assembly. The BFI system inside the cryomacrotome has been designed to be fully automated and does not add to the histotechnician's task of tape transfer based cryosectioning. In addition, the BFI and cryosectioning are spatially separated and it does not obstruct the cryosectioning.

Our system utilizes deep ultraviolet excitation which elicits autofluorescence differentially from the components of the brain tissue. The illumination is invisible to our imaging system while capturing fluorescence in our biological tissues. We believe that this differential autofluorescence elicited by different components of the brain tissue is a result of difference in the constituents such as lipofuscin, lipids, amino acids and molecular substrates such as NADPH. (for details see Croce and Bottiroli, 2014). This is evident from our images where the large white matter tracts across the human cerebellum fluoresce more than any other component of the cryoblock under the UV-C illumination. The camera and imaging system can image any visible wavelength, and thus

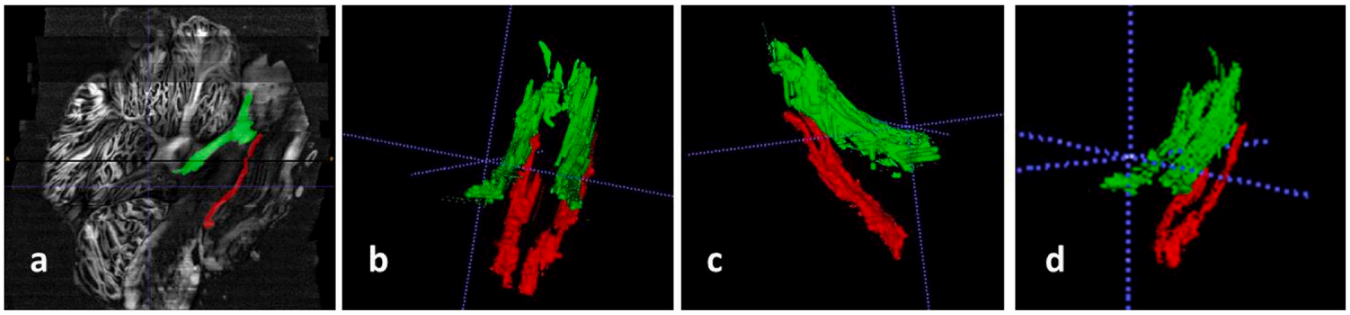

Fig. 11. shows an example of how our BFI can be used in the reconstruction of white matter pathway. (a) shows a reconstructed sagittal section where the medial lemniscus and superior cerebellar peduncles were segmented (shown in red and green respectively). (b), (c) and (d) are three dimensional segmentation masks of the two tracts shown in multiple orientations in 3D.

it can potentially be used for other tissues that exhibit different autofluorescence properties. In addition, our system can be easily adapted to image other techniques that involve tissue clearing combined with fluorescent tracer or genetically modified tissue.

There is a chance that the autofluorescence observed can be from the contributions of structures below the imaged surface. However, UV-C has lower penetration depth in human tissues as compared to other wavelengths in the spectrum. The penetration depth from previous work for similar wavelengths was found to be between 2 and 40 μm, 2 μm (Duck, 1990), 2 μm (Anderson and Parrish, 1981), < 20 μm (Meinhardt et al., 2008), 30 μm (Scientific Committee on Health, Environmental and Emerging Risks: SCHEER, 2017), 40 μm (Scientific Committee on Emerging and Newly Identified Health Risks: SCENIHR, 2012). This indicates that the contribution of underlying layers to observed fluorescence at the worst case can only be 40 μm in depth.

Our choice of the camera and its optics largely was due to the prioritization of large field of view rather than ultra-high resolution, in addition to weight considerations as described before. However, with the rapid improvements in camera design and resolution, we expect the system to be easily adaptable to future ultra-high-resolution cameras and imaging systems. With the different types of tissue formats planned, the BFI system has also been designed to be adaptable across a wide range of tissue sizes from foetal to adult human brain, by simple adjustments to the focus and working distance.

We used fluorescent fiducial markers that were attached to the surface of the cryochuck rather than the block itself. This creates a disadvantage, particularly for very large blocks during sectioning. Since the fiducial markers are mounted on the cryochuck, they are seen as undergoing enlargement as the cryosectioning proceeds.

5. Conclusions

We have designed a BFI system specifically for imaging large volume biological tissues, such as the human brains, which fit only on non-standard slide format (200 × 150 mm). There is a trade off in the BFI system between the resolution and FoV. More importantly, it provides larger field of view required for imaging the large samples such as the adult human brain. We have successfully deployed the system to work under low temperature working conditions inside a cryomacrotome. The system worked for long periods in low temperature conditions (15 days) with little or no intervention. The system was tested on an adult human cerebellum and brainstem cryoblock, resulting in the imaging of 2995 sections with no loss. The BFI system, due to its positioning on the cryomacrotome's knife holder assembly ensures that there is no need for frequent adjustments in focus or field of view during the cryosectioning process. The BFI provides an important reference and has been shown to highlight the changes undergone by the tissue after cryosectioning and staining. The use of deep ultraviolet illumination highlights salient features of the brain. Block face imaging provides a valuable resource to study a tissue sample prior to the histological processing and can be easily applied to any tissue that undergoes histology.

Funding sources

The work was funded by grants received from the Office of the Principal Scientific Adviser to the Government of India and The Pratiksha Trust. Partha Mitra and Jaikishan Jayakumar receive funding support from the HN Mahabala chair professorship in computational neuroscience of the Indian Institute of Technology Madras.

CRediT authorship contribution statement

Srinivasa Karthik: Conceptualization, Methodology, Investigation, Writing - Original Draft. **Jayaraj Joseph**: Conceptualization, Methodology, Writing - Review & Editing, Supervision. **Jaikishan Jayakumar**: Investigation, Writing - Review & Editing, Visualization. **Rahul Manoj**: Investigation, Writing - Original Draft. **Mahesh Shetty**: Methodology, Software, Validation, Investigation. **Mihail Bota:** Investigation, Writing - Review & Editing. **Richa Verma**: Investigation, Supervision, Project administration. **Partha Mitra**: Conceptualization, Supervision, Funding acquisition. **Mohanasankar Sivaprakasam**: Conceptualization, Supervision, Project administration, Funding acquisition.

Declaration of Competing Interest

The authors declare no conflict of interest.

Data availability

Data will be made available on request.

Acknowledgements

The authors would like to acknowledge our clinical collaborators from CMC Vellore for the autopsy and brain retrieval for histological processing. They would like to acknowledge the histotechnicians at SGBC for processing the biological specimen on which the developed block face imaging was tested.

Research & Ethics Statement

The study was conducted according to the guidelines approved by the Review Board and Ethics Committee of Christian Medical College Vellore (IRBNo:13262). All tissue processing was performed based on a protocol approved by the IITM Institutional Human Ethics Committee (EC/2021–01/MS/06) guidelines.

References

Alegro, M., Amaro, E., Loring, B., Heinsen, H., Alho, E., Zollei, L., Ushizima, D., Grinberg, L.T., 2016. Multimodal whole brain registration: MRI and high resolution histology. IEEE Comput. Soc. Conf. Comput. Vis. Pattern Recognit. Work 634–642. https://doi.org/10.1109/CVPRW.2016.85.

Alho, E.J.L., Alho, A.T.D.L., Grinberg, L., Amaro, E., dos Santos, G.A.B., da Silva, R.E., Neves, R.C., Alegro, M., Coelho, D.B., Teixeira, M.J., Fonoff, E.T., Heinsen, H., 2018. High thickness histological sections as alternative to study the three-dimensional microscopic human sub-cortical neuroanatomy. Brain Struct. Funct. 223, 1121–1132. https://doi.org/10.1007/s00429-017-1548-2.

Amunts, K., Lepage, C., Borgeat, L., Mohlberg, H., Dickscheid, T., Rousseau, M.É., Bludau, S., Bazin, P.L., Lewis, L.B., Oros-Peusquens, A.M., Shah, N.J., Lippert, T., Zilles, K., Evans, A.C., 2013. BigBrain: an ultrahigh-resolution 3D human brain model. Science 80 (340), 1472–1475. https://doi.org/10.1126/science.1235381.

Amunts, K., Mohlberg, H., Bludau, S., Zilles, K., 2020. Julich-Brain: a 3D probabilistic atlas of the human brain's cytoarchitecture. Science 80- (369), 988–992. https://doi.org/10.1126/science.abb4588.

Anderson, R.R., Parrish, J.A., 1981. The optics of human skin. ISSN 0022-202X J. Invest. Dermatol. 77 (1), 13–19. https://doi.org/10.1111/1523-1747.ep12479191.

Annese, J., Sforza, D.M., Dubach, M., Bowden, D., Toga, A.W., 2006. Postmortem high-resolution 3-dimensional imaging of the primate brain: blockface imaging of perfusion stained tissue. Neuroimage 30, 61–69. https://doi.org/10.1016/j.neuroimage.2005.03.043.

Appel, A.A., Anastasio, M.A., Larson, J.C., Brey, E.M., 2013. Imaging challenges in biomaterials and tissue engineering. Biomaterials 34, 6615–6630. https://doi.org/10.1016/j.biomaterials.2013.05.033.

Bouchard, M.B., Voleti, V., Mendes, C.S., Lacefield, C., Grueber, W.B., Mann, R.S., Bruno, R.M., Hillman, E.M.C., 2015. Swept confocally-aligned planar excitation (SCAPE) microscopy for high-speed volumetric imaging of behaving organisms. Nat. Photonics 9, 113–119. https://doi.org/10.1038/nphoton.2014.323.

Choe, A.S., Gao, Y., Li, X., Compton, K.B., Stepniewska, I., Anderson, A.W., 2011. Accuracy of image registration between MRI and light microscopy in the ex vivo brain. Magn. Reson. Imaging 29, 683–692. https://doi.org/10.1016/j.mri.2011.02.022.

Collins, D.L., Neelin, P., Peters, T.M., Evans, A.C., 1994. Automatic 3d intersubject registration of mr volumetric data in standardized talairach space. J. Comput. Assist. Tomogr. 18 https://doi.org/10.1097/00004728-199403000-00005.

Croce, A.C., Bottiroli, G., 2014. Autofluorescence spectroscopy and imaging: a tool for biomedical research and diagnosis. Eur. J. Histochem 58, 320–337. https://doi.org/10.4081/ejh.2014.2461.

Denk, W., Horstmann, H., 2004. Serial block-face scanning electron microscopy to reconstruct three-dimensional tissue nanostructure. PLoS Biol. 2, e329 https://doi.org/10.1371/journal.pbio.0020329.

Ding, S.L., Royall, J.J., Sunkin, S.M., Ng, L., Facer, B.A.C., Lesnar, P., Guillozet-Bongaarts, A., McMurray, B., Szafer, A., Dolbeare, T.A., Stevens, A., Tirrell, L., Benner, T., Caldejon, S., Dalley, R.A., Dee, N., Lau, C., Nyhus, J., Reding, M., Riley, Z.L., Sandman, D., Shen, E., van der Kouwe, A., Varjabedian, A., Write, M., Zollei, L., Dang, C., Knowles, J.A., Koch, C., Phillips, J.W., Sestan, N., Wohnoutka, P., Zielke, H.R., Hohmann, J.G., Jones, A.R., Bernard, A., Hawrylycz, M.J., Hof, P.R., Fischl, B., Lein, E.S., 2016. Comprehensive cellular-resolution atlas of the adult human brain. J. Comp. Neurol. 524, 3127–3481. https://doi.org/10.1002/cne.24080.

Dobbs, J., Krishnamurthy, S., Kyrish, M., Benveniste, A.P., Yang, W., Richards-Kortum, R., 2015. Confocal fluorescence microscopy for rapid evaluation of invasive tumor cellularity of inflammatory breast carcinoma core needle biopsies. Breast Cancer Res. Treat. 149. https://doi.org/10.1007/s10549-014-3182-5.

Duck, F.A., 1990. Physical Properties of Tissue. Academic Press, London, p. 1990.

Evans, Alan, C., Louis Collins, D., 1992. An MRI-based stereotactic atlas from 250 young normal subjects. The Society for Neuroscience Abstracts 18, 408.

Fereidouni, F., Wood, L., Kiemen, A., Abraham, T., Wu, P.H., Wirtz, D., Levenson, R., 2021. 3D histology of tissue using vibrating microtome block-face imaging and MUSE microscopy (3D MUSE). Opt. Info Conf. Pap. NW3C. 4. https://doi.org/10.1364/ntm.2021.nw3c.4.

Gabriele, M.L., Wollstein, G., Ishikawa, H., Kagemann, L., Xu, J., Folio, L.S., Schuman, J. S., 2011. Optical coherence tomography: History, current status, and laboratory work. Investig. Ophthalmol. Vis. Sci. https://doi.org/10.1167/iovs.10-6312.

Guo, J., Artur, C., Eriksen, J., Mayerich, D., 2019a. Three-dimensional macro-scale micro-structure imaging with deep ultraviolet excitation. Proceedings of SPIE: Advanced Optical Imaging Technologies II 11186, 23. https://doi.org/10.1117/12.2538364.

Guo, J., Artur, C., Eriksen, J.L., Mayerich, D., 2019b. Three-dimensional microscopy by milling with ultraviolet excitation. Sci. Rep. 9, 1–9. https://doi.org/10.1038/s41598-019-50870-1.

Holmes, C.J., Hoge, R., Collins, L., Woods, R., Toga, A.W., Evans, A.C., 1998. Enhancement of MR images using registration for signal averaging. J. Comput. Assist. Tomogr. 22. https://doi.org/10.1097/00004728-199803000-00032.

Ishii, N., Tajika, Y., Murakami, T., Galipon, J., Shirahata, H., Mukai, R., Uehara, D., Kaneko, R., Yamazaki, Y., Yoshimoto, Y., Iwasaki, H., 2021. Correlative microscopy and block-face imaging (CoMBI) method for both paraffin-embedded and frozen specimens. Sci. Rep. 11, 1–17. https://doi.org/10.1038/s41598-021-92485-5.

Kang, D., Carruth, R.W., Kim, M., Schlachter, S.C., Shishkov, M., Woods, K., Tabatabaei, N., Wu, T., Tearney, G.J., 2013. Endoscopic probe optics for spectrally encoded confocal microscopy. Biomed. Opt. Express 4, 1925. https://doi.org/10.1364/boe.4.001925.

Kasaragod, D., Zhu, M., Aizawa, H., 2021. Deep ultraviolet based serial block-face imaging for three dimensional morphological assessment of the rodent brains 11925, 9. https://doi.org/10.1117/12.2615413.

Lebenberg, J., Hérard, A.S., Dubois, A., Dauguet, J., Frouin, V., Dhenain, M., Hantraye, P., Delzescaux, T., 2010. Validation of MRI-based 3D digital atlas registration with histological and autoradiographic volumes: an anatomofunctional transgenic mouse brain imaging study. Neuroimage 51, 1037–1046. https://doi.org/10.1016/j.neuroimage.2010.03.014.

Lipke, E., Hörnschemeyer, T., Pakzad, A., Booth, C.R., Michalik, P., 2014. Serial block-face imaging and its potential for reconstructing diminutive cell systems: a case study from arthropods. Microsc. Microanal. 20, 946–955. https://doi.org/10.1017/S1431927614000087.

Lowe, D.G., 2004. Distinctive image features from scale-invariant keypoints. Int. J. Comput. Vis. 60, 91–110. https://doi.org/10.1023/B:VISI.0000029664.99615.94.

Lu, C.H., Tang, W.C., Liu, Y.T., Chang, S.W., Wu, F.C.M., Chen, C.Y., Tsai, Y.C., Yang, S. M., Kuo, C.W., Okada, Y., Hwu, Y.K., Chen, P., Chen, B.C., 2019. Lightsheet localization microscopy enables fast, large-scale, and three-dimensional super-resolution imaging. Commun. Biol. 2. https://doi.org/10.1038/s42003-019-0403-9.

Mai, J.K., Paxinos, G., Voss, T., 2015. Atlas of the Human Brain, 4th ed, Academic Press.

Mancini, M., Casamitjana, A., Peter, L., Robinson, E., Crampsie, S., Thomas, D.L., Holton, J.L., Jaunmuktane, Z., Iglesias, J.E., 2020. A multimodal computational pipeline for 3D histology of the human brain. Sci. Rep. 10, 1–21. https://doi.org/10.1038/s41598-020-69163-z.

Mazziotta, John C., Toga, A.W., Evans, A.C., Fox, P.T., Lancaster, J.L., 1995. Digital brain atlases. In: Trends Neurosci, 18, pp. 210–211. https://doi.org/10.1016/0166-2236(95)93904-C.

Meinhardt, M., Krebs, R., Anders, A., Heinrich, U., Tronnier, H., 2008. Wavelength-dependent penetration depths of ultraviolet radiation in human skin. J. Biomed. Opt. 13 (4), 044030 https://doi.org/10.1117/1.2957970.

Naidich, T.P., Duvernoy, H.M., Delman, B.N., Sorensen, A.G., Kollias, S.S., Haacke, E.M., 2009. Duvernoy's Atlas of the Human Brain Stem and Cerebellum, Duvernoy's Atlas of the Human Brain Stem and Cerebellum. https://doi.org/10.1007/978-3-211-73971-6.

Neil, M.A.A., Juškaitis, R., Wilson, T., 1997. Method of obtaining optical sectioning by using structured light in a conventional microscope. Opt. Lett. 22. https://doi.org/10.1364/ol.22.001905.

Orringer, D.A., Pandian, B., Niknafs, Y.S., Hollon, T.C., Boyle, J., Lewis, S., Garrard, M., Hervey-Jumper, S.L., Garton, H.J.L., Maher, C.O., Heth, J.A., Sagher, O., Wilkinson, D.A., Snuderl, M., Venneti, S., Ramkissoon, S.H., McFadden, K.A., Fisher-Hubbard, A., Lieberman, A.P., Johnson, T.D., Xie, X.S., Trautman, J.K., Freudiger, C. W., Camelo-Piragua, S., 2017. Rapid intraoperative histology of unprocessed surgical specimens via fibre-laser-based stimulated Raman scattering microscopy. Nat. Biomed. Eng. 1. https://doi.org/10.1038/s41551-016-0027.

Pichat, J., Iglesias, J.E., Yousry, T., Ourselin, S., Modat, M., 2018. A survey of methods for 3D histology reconstruction. Med. Image Anal. 46, 73–105. https://doi.org/10.1016/j.media.2018.02.004.

Pinskiy, V., Jones, J., Tolpygo, A.S., Franciotti, N., Weber, K., Mitra, P.P., 2015. High-throughput method of whole-brain sectioning, using the tape-transfer technique. PLoS One 10, 1–15. https://doi.org/10.1371/journal.pone.0102363.

Roy, D., Steyer, G.J., Gargesha, M., Stone, M.E., Wilson, D.L., 2009. 3D cryo-imaging: a very high-resolution view of the whole mouse. Anat. Rec. 292, 342–351. https://doi.org/10.1002/ar.20849.

SCENIHR (Scientific Committee on Emerging and Newly Identified Health Risks), 2012. Health effects of artificial light, report published: 19 March 2012. Eur. Union 2012. https://doi.org/10.2772/8624.

SCHEER (Scientific Committee on Health, Environmental and Emerging Risks), 2017. Opinion on Biological effects of UV C radiation relevant to health with particular reference to UV C lamps, report published: 2 February 2017. Eur. Union 2017. https://doi.org/10.2875/569379.

Schmahmann, J.D., Doyon, J., McDonald, D., Holmes, C., Lavoie, K., Hurwitz, A., Kabani, N., Toga, A., Evans, A., Petrides, M., 1999. Three-dimensional MRI atlas of the human cerebellum in proportional stereotaxic space. Neuroimage 10, 233–260. https://doi.org/10.1006/nimg.1999.0459.

Sliney, D.H., Stuck, B.E., 2021. A need to revise human exposure limits for ultraviolet UV-C radiation. Photochem. Photobio. 97, 485–492. https://doi.org/10.1111/php.13402.

Starborg, T., Kadler, K.E., 2015. Serial block face-scanning electron microscopy: a tool for studying embryonic development at the cell-matrix interface. Birth Defects Res. Part C. - Embryo Today Rev. 105, 9–18. https://doi.org/10.1002/bdrc.21087.

Tajika, Y., Murakami, T., Iijima, K., Gotoh, H., Takahashi-Ikezawa, M., Ueno, H., Yoshimoto, Y., Yorifuji, H., 2017. A novel imaging method for correlating 2D light microscopic data and 3D volume data based on block-face imaging. Sci. Rep. 7, 1–12. https://doi.org/10.1038/s41598-017-03900-9.

Takaishi, R., Aoyama, T., Zhang, X., Higuchi, S., Yamada, S., Takakuwa, T., 2014. Three-dimensional reconstruction of rat knee joint using episcopic fluorescence image capture. Osteoarthr. Cartil. 22, 1401–1409. https://doi.org/10.1016/j.joca.2014.06.016.

Mazziotta, J.C., Toga, A.W., Evans, A., Fox, P., Lancaster, J., 1995. A probabilistic atlas of the human brain: theory and rationale for its development. The International Consortium for Brain Mapping (ICBM). NeuroImage 2 (2), 89–101. https://doi.org/10.1006/nimg.1995.1012. ISSN 1053-8119. https://www.sciencedirect.com/science/article/pii/S1053811985710129.

Talairach, J., Tournoux, P., 1988. Co-planar Stereotaxic Atlas of the Human Brain: 3-dimensional Proportional System : an Approach to Cerebral Imaging. G. Thieme, Germany.

Tang, S., Zhou, Y., Ju, M.J., 2012. Multimodal optical imaging with multiphoton microscopy and optical coherence tomography. J. Biophotonics 5, 396–403. https://doi.org/10.1002/jbio.201100138.

Wilson, D., Roy, D., Steyer, G., Gargesha, M., Stone, M., McKinley, E., 2008. Whole mouse cryo-imaging. Med. Imaging 2008 Physiol. Funct. Struct. Med. Images 6916, 69161I. https://doi.org/10.1117/12.772840.

Yoshiyama, K.O., Okamoto, N.L., Hidema, J., Higashitani, A., 2023. 222 nm far-UVC efficiently introduces nerve damage in Caenorhabditis elegans. PLoS ONE 18 (1), e0281162. https://doi.org/10.1371/journal.pone.0281162.